# An assessment of image classifiers for generating machine-learning training samples for mapping the invasive *Campuloclinium macrocephalum* (Less.) DC (pompom weed) using DESIS hyperspectral imagery

Madodomzi Mafanya [a,b,d,*], Philemon Tsele [a], Tsungai Zengeya [c,d], Abel Ramoelo [a]

[a] University of Pretoria, Department of Geography, Geoinformatics and Meteorology, Pretoria, South Africa

[b] University of South Africa, Department of Geography, Pretoria, South Africa

[c] University of Pretoria, Centre for Invasion Biology, Department of Zoology and Entomology, Pretoria, South Africa

[d] South African National Biodiversity Institute, Kirstenbosch Research Centre, Cape Town, South Africa

**Keywords:** Image classifiers, training samples, pompom weed, spectral angle mapper, maximum likelihood, support vector machine, DESIS

## Abstract

Machine-learning algorithms may require large numbers of reference samples to train depending on the spatial and spectral heterogeneity of the mapping area. Acquiring these reference samples using traditional field data collection methods is a challenge due to time constraints, logistical limitations, and terrain inaccessibility. The aim of study was to assess how parametric, nonparametric, and spectral matching image classifiers can be used to generate a large number of accurate training samples from minimal ground control points to train machine-learning algorithms for mapping the invasive pompom weed using 30 m DESIS hyperspectral data. Three image classifiers, namely, maximum likelihood classifier (MLC), support vector machine (SVM) and spectral angle mapper (SAM) were selected to represent each of the three types of image classifiers under investigation in this study. Results show that the SAM, MLC and SVM classifiers had pixel-based classification accuracies of 87%, 73% and 67% for the pompom-containing pixels class, respectively. Furthermore, an independent field verification for the SAM classification was conducted yielding a 92% overall mapping accuracy for the pompom-containing pixels class. A total of 4 000 pompom-containing and 8 000 non-pompom-containing training samples were generated from an SAM classification that was trained using only 20 endmembers. Overall, this study presents a potential solution strategy that has significant implications for generating large numbers of reference training samples for mapping invasive alien plants from new generation spaceborne hyperspectral imagery using machine-learning algorithms.

## 1. Introduction

Internationally, there has been increasing efforts by the ecological science community to report on the status of biological invasions and to implement initiatives aimed at minimising their impacts on biodiversity (McGeoch *et al.,* 2010). This is for achieving the targets aimed at reducing their negative impacts on global change (Tittensor *et al.,* 2014). In South Africa, reporting on the status of biological invasions at country level, particularly the spatial distribution of invasive alien plants (IAPs), is intended to aid in policy formulation for their effective management (Wilson *et al.,* 2018). Globally, there is a scarcity of accurate information on the spatial distribution of IAPs and such geospatial information is necessary for planning their effective management and for minimising their negative environmental impacts (Kganyago *et al.,* 2018). Remote sensing has been shown to be an effective tool for collecting the necessary IAPs spatial information (Müllerová *et al.*, 2013). This spatial information is mainly derived from remotely sensed data using image classifiers (Mafanya *et al.*, 2017). These image classifiers mainly include parametric, nonparametric, and spectral matching algorithms. In particular, parametric image classifiers are either distance-based or probabilistic and their aim is to characterize an image feature space from which classes can be separated using similarity thresholds (Perumal and Bhaskaran, 2010; Silva *et al*., 2013). In contrast, nonparametric image classifiers learn directly from the training samples whereby an optimal boundary between classes is determined (Maxwell *et al*., 2018). On the other hand, spectral matching algorithms use error metrics and constraints to determine the existence of a spectral match between reference spectra and an unknown spectrum (Dennison *et al*., 2004).

The assessment of parametric and nonparametric image classifiers for mapping IAPs from hyperspectral data is usually conducted to determine the best performing classifier in realising a certain mapping objective (Bachmann *et al*., 2002; Rajapakse et al., 2006; Skowronek *et al.*, 2018). There are numerous examples of studies that assessed the performance of the aforementioned image classifiers. In particular, for parametric classifiers, Underwood *et al*., (2003) assessed the mapping accuracy of the maximum likelihood classifier (MLC) using three different hyperspectral data processing methods for detecting the invasive iceplant (*Carpobrotus edulis*) and jubata grass (*Cortaderia jubata*) from Airborne Visible/ Infrared Imaging Spectrometer (AVIRIS) data. Hamada *et al*., (2007) assessed the distance-based parallelepiped classifier for detecting the invasive tamarisk species (*Tamarix* spp.) from very high spatial resolution (0.5 m) hyperspectral data in riparian habitats of Southern California, USA. Their findings indicated that the parallelepiped classifier yielded the most accurate and

reliable tamarisk classification products. On the other hand, for nonparametric classifiers, Narumalani *et al*., (2006) assessed the mapping accuracy of the iterative self-organizing data (ISODATA) algorithm against the spectral angle mapper (SAM) in identifying salt cedar (*Tamarix* spp.) in Lake Meredith, Texas. In their study, validation procedures revealed 76% and 83% mapping accuracies for the ISODATA and SAM algorithms, respectively. Moreover, Lawrence *et al*., (2006) assessed the mapping accuracies of the random forest (RF) algorithm for classifying leafy spurge (*Euphorbia esula* L.) and spotted knapweed (*Centaurea maculosa* Lam.) in North American rangelands. They reported an overall mapping accuracy of 86% which was a substantial improvement in accuracy compared to single classification trees. Correspondingly, the support vector machine (SVM) classifier was used to detect the noxious weed *Carduus nutans* (musk thistle) in its different phenological stages using AISA hyperspectral imagery (Mirik *et al*., 2013). In addition, Sabat-Tomala *et al*., (2020) assessed the SVM against the RF in identifying *Solidago* spp, *Calamagrostis epigejos*, and *Rubus* spp. from HySpex airborne hyperspectral imagery in Malinowice, Poland. The assessment of spectral matching algorithms for mapping IAPs using hyperspectral data is usually done in comparison with other image classifiers. For instance, Ustin *et al*., (2002) compared the SAM and MLC classifiers for mapping the invasive *Arundo donax* (giant cane) yielding overall accuracies of 91% and 98% for the SAM and MLC, respectively.

High quality training samples are essential for large-scale supervised landcover mapping (Huang et al., 2020). Moreover, best practices in image classification suggest that supervised image classifiers require a certain minimum number of reference samples to train and this number depends on the type of the algorithm being utilised (Huang *et al*., 2002). For parametric classifiers, the 'rule of thumb' is that the minimum number of reference training samples should be 10 times the number of variables under study (Maxwell *et al*., 2018). For nonparametric classifiers, however, there is no consensus in literature regarding the recommended minimum number of reference training samples and this number may depend on the size and spatial variability of the mapping area and (or) the algorithm to be utilised for image classification (Huang *et al*., 2002). For example, Sabat-Tomala *et al*., (2020) tested 30, 50, 100, 200 and 300 reference training pixels per class and found that fewer reference training pixels resulted in lower mapping accuracies for both SVM and RF algorithms. Meaning large numbers of accurate training samples are necessary for training machine-learning (ML) algorithms (Yu *et al*., 2022). The requirement of large numbers of accurate training samples has also been demonstrated in the application of deep convolutional spectral-spatial networks on

hyperspectral images. For instance, the spectral-spatial residual network (SSRN) and the fast and dense spectral-spatial convolutional network (FDSSC) achieved accuracies higher than 98%, when the number of training samples was more than 800 but achieved less than 90% when the number of training samples was 200 (Wang *et al*., 2019). In general, machine-learning algorithms may require hundreds to thousands of reference samples to train depending on the spatial and spectral heterogeneity as well as the size of the mapping area (Huang *et al*., 2002). For instance, Melgani and Bruzzone (2004) used 4757 training and 4588 validation samples to achieve valid and effective SVM classification results from hyperspectral remotely sensed imagery. Moreover, for convolutional neural networks (CNNs), Chen *et al*., (2019) used 6090 training samples for assessing the performance of a Fletcher-Reeves CNN (F-R CNN) against a traditional CNN model. However, acquiring thousands of accurate reference training samples using traditional field data collection methods such as the Global Navigation Satellite System (GNSS), may be impractical due to time constraints, logistical limitations, and terrain inaccessibility (Fang *et al*., 2020; Huang *et al*., 2021).

The efforts at assessing parametric, nonparametric, and spectral matching algorithms to determine the best performing image classifiers for mapping IAPs have been made. Hence the current study assessed the mapping accuracies of SAM, MLC and SVM algorithms for generating thousands of accurate samples for training machine-learning algorithms to map the invasive *Campuloclinium macrocephalum* (Less.) DC (commonly known as 'pompom weed') in a heterogeneous urban landscape using hyperspectral imagery from the recently commissioned DESIS sensor. The machine-learning algorithms and the deep learning CNN approaches are employed in subsequent pompom mapping experiments in this series of case studies because ML allows for the migration of training samples to sites not previously visited while CNNs can also better handle intra-class spectral variability and spatial heterogeneity during image classification for plant species specific mapping (Huang *et al*., 2020; Hu *et al*., 2022). Overall, this study presents a potential solution strategy that could have significant implications in generating large numbers of accurate training samples for mapping IAPs in heterogenous environments from new generation spaceborne hyperspectral imagery using machine-learning algorithms.

## 2. Study area and species description

### 2.1.Study area

The chosen study area is located south of Pretoria, the capital city of South Africa, which is situated in Gauteng, the most densely populated province (~785/km$^2$) of the country (Figure 1b). At the center of the study area is Centurion, which is a highly developed urban area characterized by a dense spatial distribution of commercial and residential buildings (Figure 1a). Furthermore, in the south-east part of the study area is the Rietvlei Nature Reserve (shown using a green boundary) that includes the Rietvlei Dam and adjacent undisturbed protected grasslands and wetlands (Figure 1a). The study area is a heterogeneous urban landscape in terms of land use and land cover types and is characterised by industrial areas, wastelands, highway roads, rail tracks as well as aviation restricted military zones. The total study area is about 393 km$^2$ with a measured average elevation of about 1 500 m above mean sea level. The study area falls within the summer rainfall region of South Africa with a minimum winter (July) rainfall amount of 6 mm and a maximum summer (January) rainfall amount of 128 mm (Kruger and Nxumalo, 2017). The area is characterised by a warm temperate climate with winter and summer average temperatures of 11 °C and 22 °C, respectively (Kruger and Shongwe, 2004).

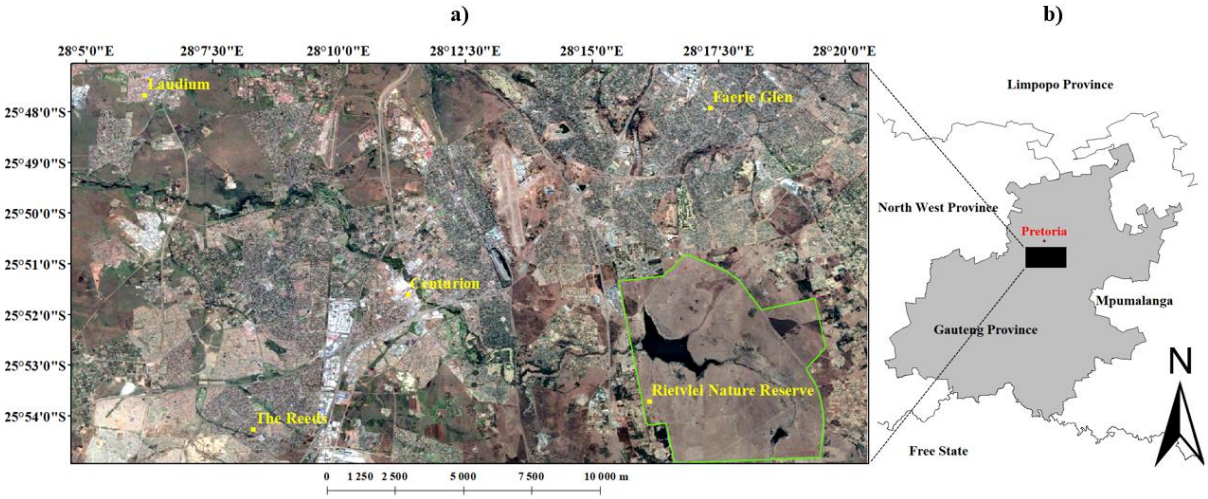


Figure 1: a) Orthorectified Google Earth image of the study area showing both developed urban areas and open grasslands and b) location of the study area relative to Pretoria and the provinces that surround the Gauteng province.

### 2.2. Species description

Pompom weed (*Campuloclinium macrocephalum* (Less.) DC) belongs to the daisy family (Asteraceae) and is native to Central and South America (Gitonga *et al*., 2015). The plant is an erect perennial herb with bright fluffy pink pom-pom like flowerheads on green stems that can grow as tall as 1.3 m high (McConnachie *et al.*, 2011). In terms of phenology, the flowering season of the pompom weed starts in Spring (October) and senescence is in Autumn during April (Goodall *et al.*, 2011). In terms of spatial distribution, pompom weed occurs in 7 out of the 9 provinces of South Africa. The pompom weed is an established invasive species in the Gauteng province, where the study area is located and an emerging weed in Mpumalanga, Limpopo, North West, KwaZulu-Natal, Free State and Eastern Cape provinces (Goodall, 2011). In particular, the provinces that surround the Gauteng Province (Figure 1b) are affected by pompom weed invasion. This is because these provinces are home to grassland and savanna biomes and pompom weed has been reported to invade mostly grasslands and open savannas (Goodall *et al.*, 2011). In terms of spread pathways, the pompom weed spreads mainly through wind dispersal and is thought to be also transferred by motor vehicles through pollens in mud stuck on car wheels (Goodall, 2016). Humans, together with freely ranging animals are also thought to be carriers of pompom weed seeds through human behaviour of flower picking as well as seeds trapped on animal fur (McConnachie *et al.*, 2011).

## 3. Datasets, image classification and validation methods

### 3.1. Methodology workflow

Represented in Figure 2 below is the methodology followed in this study.

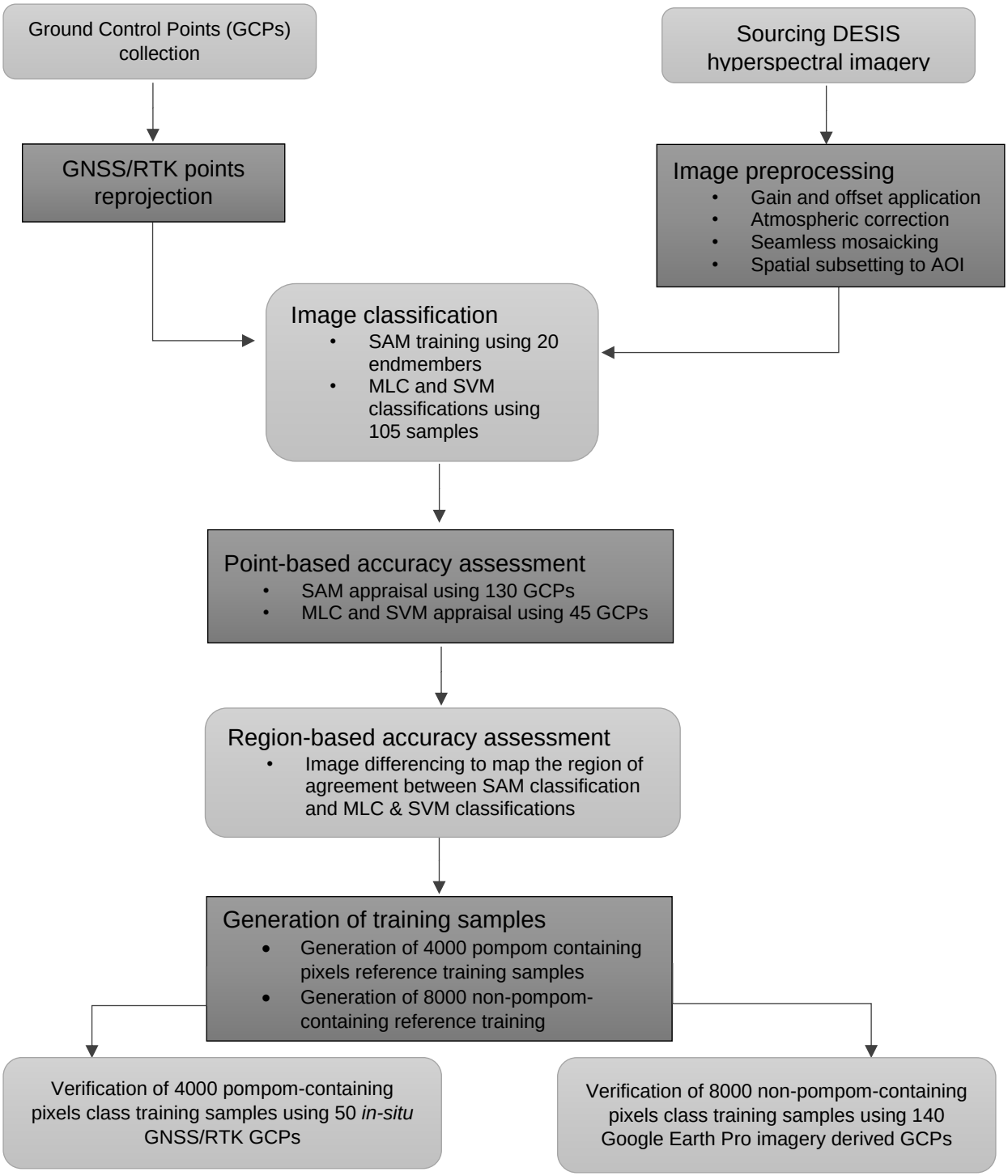


Figure 2: Workflow for generating and validating large numbers of training samples for mapping the invasive pompom weed using field data and DESIS hyperspectral imagery.

### 3.2.Training and validation data

Ground control points (GCPs) were recorded using a Global Navigation Satellite System (GNSS) operated in Real Time Kinematic (RTK) mode. The RTK connection was achieved through the South African TrigNet network of 63 continuously operating GNSS base stations that are spread throughout the country to provide RTK corrections to roving GNSS receivers in real time (Hedling *et al.,* 2000). To obtain high precision GNSS positions, operational tolerances were set to 2 mm and 3 mm for the horizontal and vertical observables, respectively. A total of 150 GCPs were recorded as reference points that contain pompom weed. Precautions were taken to ensure that each GCP was taken at the center of a pompom weed cluster larger than 10 m x 10 m in size as opposed to isolated weeds. In addition, 250 reference points that do not contain pompom weed were collected from Google Earth imagery. Priori knowledge was used to collect reference points that do not contain pompom weed on the basis that pompom weed invades grasslands and therefore the non-pompom-containing GCPs were collected on targets such as buildings, tar roads, water bodies, sport fields and golf courses. These data were then split into training and validation datasets for the SAM, MLC and SVM classification methods. For the SAM classification, a set of 20 reference points was used to create input endmembers while 130 points were withheld for validation. For the MLC and SVM classifications, reference data were divided into 70% and 30% training and validation data, respectively, where 105/150 pompom reference points were used for training and 45/150 pompom-containing points were used for validation in a 70:30 ratio. In addition, 175/250 non-pompom-containing points were used for training the non-pompom class and 75 non-pompom containing points were used for validating MLC and SVM classifications while no non-pompom endmembers were required for the SAM classification.

### 3.3. DESIS hyperspectral data

#### 3.3.1. Data description

The hyperspectral data was obtained from the German Aerospace Center (abbreviated as DLR in the German name) through a Teledyne Brown Engineering (TBE) tasking request of the DESIS hyperspectral sensor on-board the International Space Station (ISS). The DESIS sensor was launched in 2018 and is a pushbroom imaging spectrometer with 1024 across track pixels of 30 m spatial resolution at nadir from an ISS altitude of 400 km (Alonso *et al.*, 2019). The instrument is spectrally sensitive over the visible and near infrared (VNIR) wavelengths of the electromagnetic spectrum and measures 235 spectral bands between 400 and 1000 nm at a

spectral resolution of 2.55 nm (Müller *et al.*, 2016). The DESIS hyperspectral sensor was tasked to obtain imagery over the study area on 15 March 2020 corresponding to the late flowering season of the pompom weed (Goodall *et al.*, 2011).

#### 3.3.2. Data pre-processing

Data were pre-processed to product level 2A as per European Space Agency (ESA) product definitions prior to delivery. The pre-processing involved; (1) spectral resampling through band binning, (2) radiometric calibration from Top of Atmosphere (TOA) radiance to ground surface reflectance and, (3) geometric calibration through earth positioning and orthorectification (Müller *et al.*, 2016). For spectral resampling, an on-board programmable band binning was applied using a scale factor of 4 to aggregate the raw 235 spectral bands into 60 bands of 10.21 nm bandwidth as outlined in Müller *et al.,* (2016). For the radiometric calibration, the gain and offset values of 0.0001 and 0.0 were applied to scale image digital numbers (DNs) to surface reflectance values between 0.0 and 1.0 using the ENVI software radiometric calibration tool (ENVI version 5.5., Exelis Visual Information Solutions, Boulder, Colorado). The delivered tiled data was then mosaicked and cropped to the 393 $km^2$ study area vector for image classification.

### 3.4. Description of the image classification methods

#### 3.4.1. Spectral angle mapper image classification

The SAM method was selected to represent the spectral matching algorithms in this study because SAM has been extensively assessed for mapping a variety of IAPs from spaceborne hyperspectral imagery (Ustin *et al*., 2002, Narumalani *et al*., 2006, Lawrence *et al*., 2006, Sahithi *et al*., 2019; Kazmi *et al*., 2021). The SAM method exploits target object spectral properties to identify similar objects in hyperspectral data cubes. In particular, the reflectance spectrum of the target object is used to classify unknown pixels by determining the similarity between the reflectance spectrum of the target and that of an unknown image pixel (Kruse *et al.*, 1993). This is achieved by treating the reference target reflectance spectrum, referred to as the endmember, and the unknown pixel reflectance spectrum as vectors in an *n*-dimensional space where *n* is equal to the number of image bands in a hyperspectral data cube (Nidamanuri and Zbell, 2011). The spectral angle between the reference target spectrum and the reference spectrum of the unknown pixel is calculated by taking the arc cosine of the dot product of the reference spectrum and the unknown spectrum. The SAM determines the similarity of an unknown spectrum *u* to a reference spectrum *r* by applying the following equation;

$$\cos^{-1}\left(\frac{\sum_{i=1}^{nb} u_i r_i}{\left(\sum_{i=1}^{nb} u_i^2\right)^{1/2}\left(\sum_{i=1}^{nb} r_i^2\right)^{1/2}}\right) \quad (1)$$

where nb is the number of bands (Kruse *et al.*, 1993) . The smaller the spectral angle, the higher the similarity between the reference target reflectance spectrum and the reflectance spectrum of the unknown pixel. During the SAM classification, pixels further away from the reference spectrum vector than a specified maximum angle threshold in radians are not classified (Kutser and Jupp, 2006). In this study, the maximum threshold angle between the endmember spectrum vector and the unknown pixel spectrum vector used was 0.1 radians as applied in (Dennison, Halligan and Roberts, 2004). For training, a set of 20 target reference spectra endmembers were extracted from 20 pompom-containing pixels that were digitized as regions of interest (ROIs) in the ENVI software based on 20 GNSS-RTK observed GCPs. Endmembers were extracted directly from the hyperspectral data cube because research has shown that endmembers extracted directly from imagery perform best as opposed to *in situ* or laboratory-derived endmembers (Jiang, van der Werff and van der Meer, 2020). The DESIS image-derived spectral plots of the 20 samples used as endmembers to train the SAM are shown in Figure 3b with Figure 3a showing the hyperspectral data cube of the Rietvlei Dam, parts of Rietvlei Nature Reserve and the surrounding urban area.

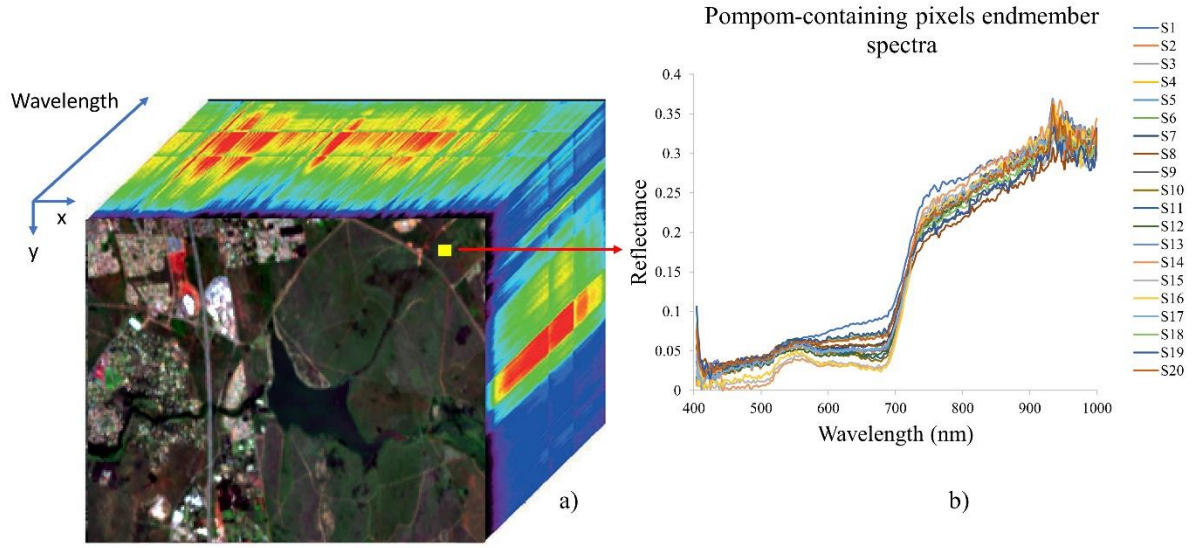

Figure 3: a) Hyperspectral data cube for a subset of the Rietvlei Nature Reserve and the surrounding urban area and b) Spectral plots of the 20 samples used as SAM endmembers.

### 3.4.2. Maximum likelihood image classification

The MLC method was selected to represent parametric classifiers in this study because MLC has been previously compared to the SAM method for mapping IAPs from hyperspectral imagery (Ustin *et al.*, 2002; Miao *et al.*, 2011). The MLC method is based on the Bayes' theorem and holds that the probability (P) that a pixel with mean vector (ω) belongs to class *i* is given by;

$$P(i|\omega) = \frac{P(\omega|i)P(i)}{P(\omega)} \quad (2)$$

where $P(\omega|i)$ is the likelihood function, $P(i)$ the probability that class *i* belongs in the image being considered and $P(\omega)$ is the probability that ω is observed (Dougherty, Newell and Pelz, 1992). Thus, a theoretical pixel *x* is assigned to class *i* using the following decision rule;

$$x \in i \quad \text{if } P(i|\omega) > P(j|\omega) \text{ for all } j \neq i \quad (3)$$

meaning pixel *x* is the element of class *i* given that the probability of pixel *x* belonging to class *i* is greater than the probability of pixel *x* belonging to class *j* where *i* is not *j* (Strahler, 1980).

Moreover, the MLC algorithm assumes that the digital numbers of a class in the image bands are normally distributed and calculates the probability of each pixel belonging to that class (Yang *et al*., 2011). The classifier considers the mean and covariance vectors of the training areas and subsequently each class is characterised by a mean vector and a covariance vector. Each image pixel is then assigned to the class for which it has the highest probability of membership (Silva *et al*., 2013). During the MLC classification, pixels whose probability of membership is below a specified probability threshold are left unclassified (Foody *et al.*, 1992). In this study, the classification probability threshold was set to 0.95. The training of the supervised MLC was done using 105 pompom-containing 30 x 30 m ROIs for the pompom class and 175 non-pompom-containing 30 x 30 m ROIs for the non-pompom classes. Furthermore, validation was done using 45 pompom-containing 30 x 30 m ROIs and 75 non-pompom containing 30 x 30 m ROIs, meaning that a 70:30 training: validation ratio was used for the MLC classification.

### 3.4.3. Support vector machine image classification

The SVM is a machine-learning classification method derived from statistical learning theory and separates classes by maximizing the margin between them using a hyperplane decision surface (Mountrakis *et al*., 2011). The SVM was selected to represent nonparametric machine learning algorithms in this study because SVM has a low sensitivity to high dimensionality and been previously assessed for species-specific mapping of IAPs from spaceborne hyperspectral data (Melgani and Bruzzone, 2004; Mirik *et al*., 2013; Sahithi *et al*., 2019; Sabat-Tomala *et al*., 2020). The classification problem in SVM involves defining this optimal decision surface (Zhu and Blumberg, 2002). The aim is to develop a model which predicts the target values of the test data using finite training data. Support vectors are the training data points that constrain the width of the hyperplane margin (Oommen *et al*., 2008). Given a training set of instance-label pairs ($x_i$,$y_i$), $i = 1,\ldots,l$ where $l$ is the number of samples, $x_i \in R^N$ is an $N$-dimensional space and, $y \in \{1,-1\}^l$ is class labels in the binary classification, the support vector machines require the solution of the following optimization problem;

$$\min_{w,b,\xi} \quad \frac{1}{2} w^T w + C\sum_{i=1}^{l} \xi_i \tag{4}$$

subject to constraints,

$$y_i(w^T \varphi(x_i) + b) \geq 1 - \xi_i \quad \xi_i \geq 0, \quad i = 1, \ldots, N \tag{5}$$

where training vectors $x_i$ are mapped into a high dimensional space (i.e. $l$ – 1 dimensions) by the function $\varphi$, $\xi$ indicates the distance of incorrectly classified points to a non-linear hyperplane and $C$ is the penalty parameter (Kavzoglu and Colkesen, 2009). In this study, the penalty parameter was set to 50 to optimize the trade-off between forcing rigid hyperplane margins and allowing training errors. Moreover, the kernel function used was the radial basis function (RBF) because of its inherent high model convergence speed and ability to produce accurate results (Zhu and Blumberg, 2002; Kavzoglu and Colkesen, 2009). The RBF kernel function is defined as follows;

$$K(x_i, x_j) = exp(-g \| x_i - x_j \|^2), \; g > 0 \tag{6}$$

where $g$ is the kernel function parameter. During the SVM classification, pixels whose probability of membership is below a specified classification probability threshold are left

unclassified. In this study, the classification probability threshold was set to 0.95, consistent with the MLC classification. The training of the supervised SVM was done using 105 pompom-containing 30 m x 30 m ROIs for the pompom class and 175 non-pompom-containing 30 x 30 m ROIs for the non-pompom class. Furthermore, the validation was done using 45 pompom-containing 30 x 30 m ROIs and 75 non-pompom-containing 30 x 30 m ROIs, meaning that a 70:30 training: validation ratio was used for the SVM classification, consistent with the MLC classification.

### 3.5. Accuracy assessment

#### 3.5.1. Pixel-based accuracy assessment

For the SAM classification, the pixel-based accuracy assessment used 130 withheld pompom-containing reference pixels to assess whether a reference pixel was classified as pompom-containing or misclassified. For the MLC and SVM classifications, 45 withheld reference pixels as per the 70:30 training: validation ratios were assessed as to whether they match pixels classified as pompom-containing or were misclassified. A table was then drawn up to count the number of correctly classified and misclassified reference pixels, respectively. Pixel-based accuracy assessment can be biased or can unfairly underestimate the accuracy of image classification in remote sensing (Foody, 2008). In addition to the pixel-based accuracy assessment, this study adopted region-based accuracy assessment procedures as outlined in the subsections below.

#### 3.5.2. Region-based accuracy assessment

Qualitative region-based accuracy assessment that is based on visual interpretation is a widely used classification validation method (Costa *et al.,* 2018). The region-based accuracy assessment compared the classification results of the SAM classifier with the classification results of the MLC and SVM methods. Firstly, a hotspots map based on high density pompom classifications was generated for the SAM classifier. A set of 8 regions consisting of 4 circles (named C1, C2, C3 & C4) and 4 ellipses (named E1, E2, E3 & E4) were created around the high-density pompom classification regions to compute the number of pixels classified as pompom-containing by the respective classifiers within these hotspots. The area of pixels classified as pompom-containing within these 8 regions was calculated to assess the area percentage of pixels classified as pompom-containing within these hotspots for each classifier. However, these area percentages lacked a spatial component as they did not show which pixels

were classified as either pompom-containing or non-pompom-containing in agreement with the SAM. This study then analysed the regions of classification agreement between SAM and MLC as well as between SAM and SVM both quantitatively and qualitatively using image differencing.

#### 3.5.3. Analysis of classification regions of agreement

To add a spatial component to the area percentages calculated in 3.4.1 and to map classification regions of agreement between the SAM and MLC as well as SAM and SVM, use of image differencing was made. Two difference images were generated by subtracting the classification images of MLC and SVM from the SAM classification image. Moreover, to further investigate the level of agreement between SAM classification results and the classification results of MLC and SVM, the 8 hotspots were cropped out of the difference images and juxtaposed next to each other at the same scale and resolution. This allowed for qualitative analysis of the classification regions of agreement. In addition to the qualitative analysis, area percentages of the regions of agreement between SAM classification results and classification results of the MLC and SVM classifiers were calculated. As part of this quantitative analysis, area percentages of mutually exclusive classification results where the SAM classified pixels as pompom-containing while the classifier in comparison classified those pixels as non-pompom-containing were calculated. The subsection below outlines an independent verification survey that was conducted post-classification.

### 3.6. Generation of training samples

The SAM classified image consisted of the pompom-containing and the non-pompom-containing pixels classes, as class 0 and Class 1, respectively. The output raster was split into two based on colour values (i.e., binary classification of class 0 ‘pompom containing’ and class 1 ‘non-pompom-containing’ where RGB values were (0,0,0) for class 0 and (255,255,255) for class 1. To generate the training samples for the pompom-containing pixels class, the SAM pompom-containing pixels raster (i.e., class 0) was vectorised into 30 m x 30 m square polygons as per spatial resolution of the DESIS hyperspectral imagery. Since machine-learning training datasets are usually administered in point-form as reference GCPs, centroids for each 30 m x 30 m square polygon were generated to create the same number of points as the number of input pixels. For the non-pompom-containing class, the class 1 raster was vectorised and then the resultant polygons were merged into one super-polygon to form the non-pompom-containing pixels superclass. A set of 8000 random points that are, at least, 100 m apart were

then generated to create non-pompom-containing training samples for subsequent machine-learning classifications. The next subsection describes the verification methods used for the generated pompom-containing and non-pompom containing training samples, respectively.

### 3.7.Verification of training samples

For the pompom-containing pixels class, an *in-situ* GNSS/RTK verification survey was conducted in areas that were not previously visited during the initial collection of reference GCPs. In particular, the Rietvlei Nature Reserve and surrounding areas within the study area were used to select 50 pixels classified as pompom-containing. The centroids of the selected pixels were visited verify whether there was pompom weed at those selected sites. This verification involved staking out to the position of each pixel of interest and checking whether there is pompom weed as per SAM classification results or there has been an error of commission. It should be noted that this verification survey was conducted in early September, a time which coincides with widespread wildfires in South Africa (Forsyth *et al.*, 2010). As a result of wildfires, some areas within the study area could not be used for the pompom-containing training samples verification as grass in those regions was burnt out.

For verifying the non-pompom-containing training samples, a grid of 28 4 m X 4 m tiles over and around the study was generated. Subsequently, four non-pompom-containing training pixels were picked proximal to the four corners and one at the centre (i.e., 5 points per tile) totalling 140 training samples for validation. The 140 samples were then verified in Google Earth Pro by zooming to each point to confirm whether it belongs to the non-pompom containing pixels class. Priori knowledge was used to assess whether a point belongs to the non-pompom-containing pixels class. For instance, points falling on the Rietvlei Dam, highway roads, private golf courses, building rooftops, industrial buildings, open-cast mines and residential estates were, without doubt, deemed as belonging to the non-pompom containing pixels class whereas points falling in open grasslands could not be verified as belonging to the non-pompom-containing pixels class. The next section presents and discusses the study findings focusing on accuracy assessment, the classification agreement between SAM and the MLC and SVM methods, results of the generation of training samples as well as the results of the verification of the resultant training samples.

## 4. Results and Discussion

### 4.1. Pixel-based accuracy assessment

Results of the pixel-based accuracy assessment indicated that the SAM method had 87% classification accuracy for the pompom-containing pixels class (Table 1). This assessment was based on 130 withheld pompom-containing reference pixels where 17 pixels (i.e. 13%) were misclassified (Table 1). In addition, the MLC and SVM methods had 73% and 69% pompom classification accuracies and misclassification of 27%and 31%, respectively. It is worth noting that all the utilized classifiers had 0% commission error for the pompom class but this could be attributed to the fact that the 250 non-pompom-containing pixels were deliberately collected over targets that are known to be spectrally dissimilar to the pompom weed (i.e. buildings, tar roads, water bodies, sport fields and golf courses). It should also be noted that all the 250 non-pompom-containing pixels were used for the SAM commission error assessment whereas only 75 non-pompom-containing pixels were used for the MLC and SVM commission error assessments. These findings suggest that the SAM classification had the highest pixel-based classification accuracy. In comparison, Ustin *et al.*, (2002) obtained 91% and 98% overall classification accuracies for mapping the invasive *Arundo donax* using SAM and MLC, respectively. The high accuracies obtained in Ustin *et al.*, (2002) could be attributed to the fact that high spatial resolution airborne AVIRIS data (~4 m) were used compared to the spaceborne 30 m DESIS spatial resolution used in this study. Subsequent analysis uses the SAM classification as a reference in comparison to the classification results of the two remainder classifiers (i.e. MLC and SVM).

Table 1: Pixel-based accuracy assessment results for the SAM, MLC and SVM classification methods

| | Number of reference pixels | Classified pixels | Percentage | Misclassified pixels | Percentage |
|---|---|---|---|---|---|
| SAM | 130 | 113 | 86,92 | 17 | 13,08 |
| MLC | 45 | 33 | 73,33 | 12 | 26,67 |
| SVM | 45 | 31 | 68,89 | 14 | 31,11 |

### 4.2. Region-based accuracy assessment

#### 4.2.1. SAM high density pompom-containing classification regions

The 8 hotspots (circles C1, C2, C3& C4 and ellipses E1, E2, E3& E4) are superimposed on a Sentinel 2 colour image of the study area in Figure 3a. The results in Figures 3b, 3c and 3d show pompom classification results for the SAM, MLC and SVM methods, respectively, with the 8 hotspots superimposed. The SAM classification results in Figure 3b showing dense clusters of pompom-containing pixels in ellipses E1, E2, E3& E4 are interesting as these regions were not visited during the initial reference data collection and had to be verified using E1, E2, and C4 during an independent verification survey. Results in Figure 3c show that the MLC classified few pixels as pompom-containing within these hotspots except for circle C3 and ellipse E4. However, results in Figure 3c show that the SVM classified many pixels as pompom-containing pixels all over the entire study area, especially around wet grassy areas and rivers. When taking into consideration only ellipse E4, it is observable that the SAM and MLC methods agree within this region whereas the SVM classified very few pixels as pompom-containing within ellipse E4. In addition to the visual analysis, area percentages of pixels classified as pompom-containing by the respective classifiers within these regions are presented and discussed in subsection 4.2.2 below.

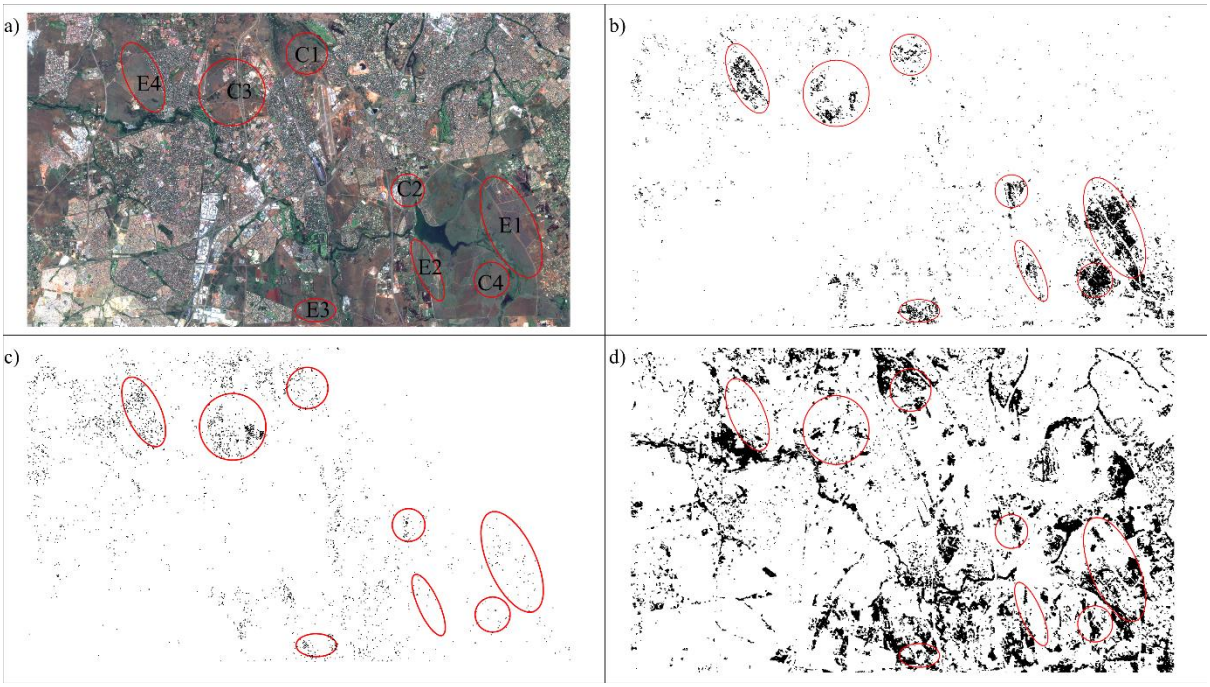


Figure 4: a) Sentinel 2 backdrop image with the 8 hotspots superimposed, b) SAM classification, c) MLC classification and d) SVM classification.

#### 4.2.2. Area calculations within SAM high density pompom classification regions

Results in Table 2 were generated by calculating the area of pixels classified as pompom-containing in Figures 4b, 4c and 4d within the 8 SAM hotspots. Table 2 shows that SAM classified pompom-containing pixels within these regions with area percentages ranging from 7.79% for C3 to 57.37% for C4. However, the MLC method area percentages ranged from 0.72% for E2 (SAM had 12.09%) to 6.04% for E4 (SAM had 17.64%). On the contrary, the SVM method area percentages ranged from 5.20% for E4 (SAM had 17.64%) to 33.00% for C1 (SAM had 9.27%). This demonstrates very large differences between the SAM and SVM classifications. Moreover, the MLC method had a classification area percentage of 0.77% for C4 as opposed to 57.37% and 22.41% for the SAM and SVM methods, respectively. The high percentage of SAM classified pompom-containing pixels in region C4 is observable from Figure 4b as a dense classification of black pixels. However, C4 contains very few black pixels in Figure 4c for the MLC classification. Contrarily, C4 contains a fair number of black pixels in Figure 4d for the SVM classification which could be attributed to the wetlands in and around C4 and the proximity to a water body that is located south-east of C4. These quantitative differences within the 8 SAM hotspots mean that neither MLC nor SVM can be used to verify the SAM classification results. The area percentages in Table 2 are presented using a bar graph in Figure 5 to further contrast the differences in the classification results of the utilised image classifiers.

Table 2: Area percentages for SAM, MLC and SVM classification methods

| | | SAM | | MLC | | SVM | |
|---|---|---|---|---|---|---|---|
| ID | Total Area (m2) | Area ($m^2$) | Percentage | Area ($m^2$) | Percentage | Area ($m^2$) | Percentage |
| C1 | 3078918 | 285300 | 9,27 | 103500 | 3,36 | 1016100 | 33,00 |
| C2 | 1946145 | 325800 | 16,74 | 42300 | 2,17 | 308700 | 15,86 |
| C3 | 8014694 | 624600 | 7,79 | 484200 | 6,04 | 802329 | 9,98 |
| C4 | 2216647 | 1271700 | 57,37 | 17100 | 0,77 | 496800 | 22,41 |
| E1 | 9374620 | 2887200 | 30,80 | 64800 | 0,69 | 2592043 | 27,65 |
| E2 | 2508141 | 303300 | 12,09 | 18000 | 0,72 | 225953 | 9,01 |
| E3 | 1681234 | 483300 | 28,75 | 78300 | 4,66 | 607075 | 36,11 |
| E4 | 4627248 | 816300 | 17,64 | 288900 | 6,24 | 240765 | 5,20 |

### 4.2.3. Area percentages within the 8 SAM high pompom density classification hotspots

The results in Table 2 were plotted on a bar graph to highlight the differences in the classification of pompom-containing pixel percentages by the respective classification methods as shown in Figure 5 below. It is observable from Figure 5 that the pompom-containing pixels were classified differently by these methods except for region C3 where all the respective area percentages were comparable. Moreover, the high SAM classification area percentage in C4 was not reciprocated by the MLC and SVM methods. In general, the MLC method classified low area percentages of pompom-containing pixels in regions C4, E1 & E2 (i.e. less than 1%) as observable in Figure 4c and Figure 5. The poor detection of pompom-containing pixels by the MLC could be attributed to the fact the training data used was insufficient as only 105 GCPs of 30 $m^2$ pixels totaling an area of 3.15 $km^2$/ 393 $km^2$ was used because in general, MLC is a robust classifier for mapping IAPs from hyperspectral imagery provided sufficient training data (Ustin *et al.*, 2002; Lawrence *et al.*, 2006). In contrast, the SVM produced higher area percentages than the SAM in regions C1 and E3 even though these circles and ellipses were generated based on SAM high pompom density classification regions. Again, the high SVM area percentages can be attributed to the fact that both C1 and E3 are in or close to wetlands and riparian areas. In addition to the insufficient training data, the poor classification accuracy by the SVM in this study can be attributed to the fact that SVM uses a pattern vector to classify objects based on pattern recognition including texture whereas the pompom weed does not form patterns as planned structures such as building structures do (Mountrakis *et al.*, 2011). Instead, the pompom weed, due to its bright pink colour, gives a distinct spectral signature, hence the SAM method performed best for classifying pompom-containing pixels in this study.

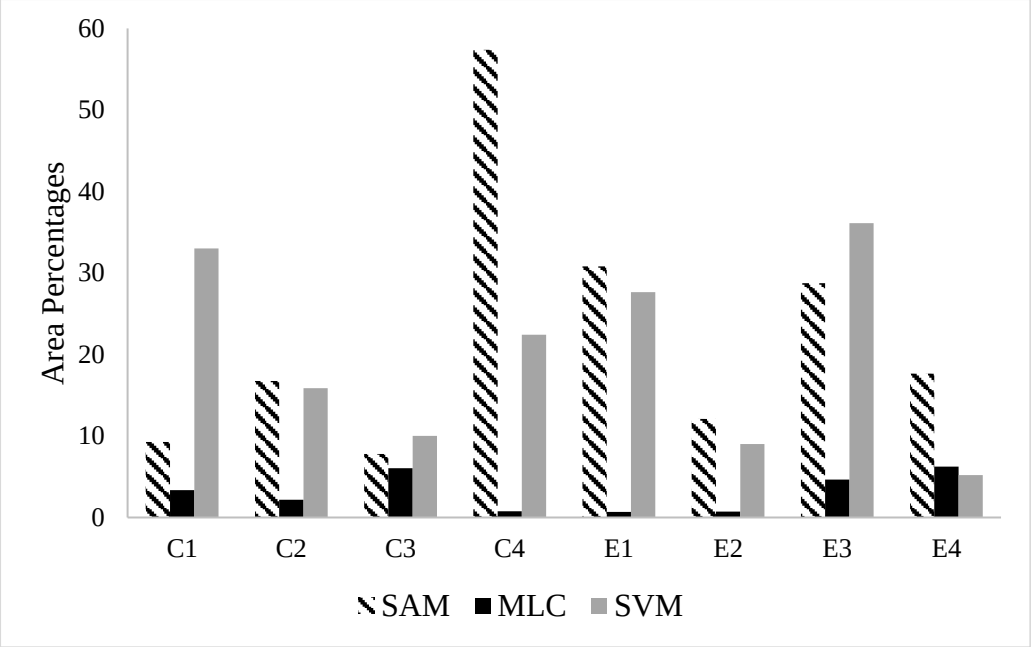


Figure 5: Quantitative differences in pompom classification area percentages for the SAM, MLC and SVM methods across the C1-C4 circles and E1-E4 ellipses of SAM high pompom density classification.

### 4.3. Classification regions of agreement

#### 4.3.1. Qualitative analysis

Results in Figure 6a is the difference image between SAM and MLC classifications whereas Figure 6b shows the difference image between SAM and SVM classifications. The white areas are regions of classification agreement and therefore the SAM and MLC generally agreed more than the SAM and SVM classifications as there is more white areas in Figure 6a than there is in Figure 6b. The black areas are pixels classified as pompom-containing by the SAM but not the classifier in comparison. The grey areas are regions classified as pompom-containing by the classifier in comparison but classified as non-pompom-containing by the SAM. It is observable from Figure 6a that the SAM method generally classified more pixels as pompom-containing than MLC as depicted on the bar graph in Figure 5 and this observation is consistent with the low classification percentages of pompom-containing pixels classified by MLC in subsection 4.2. However, the SVM classified more pixels as pompom-containing than SAM in Figure 6b, as depicted by large grey areas especially in and around rivers and wetlands. In general, there is fewer grey areas in Figure 6a than there is in Figure 6b meaning that the MLC rarely classified pixels as pompom-containing that were not classified as such by the SAM method. Finally, the SAM high density classification regions of circles and ellipses were

juxtaposed in Figures 6c and 6d for a clearer qualitative analysis to show the level of agreement or disagreement within these regions. The results in Figures 6c and 6d show that the MLC and SVM classifications were not qualitatively similar to the SAM classification within the 8 hotspots. The overall study area classification agreement results were quantitatively summarised using Tables 3 and 4 as presented and discussed in the next subsection.

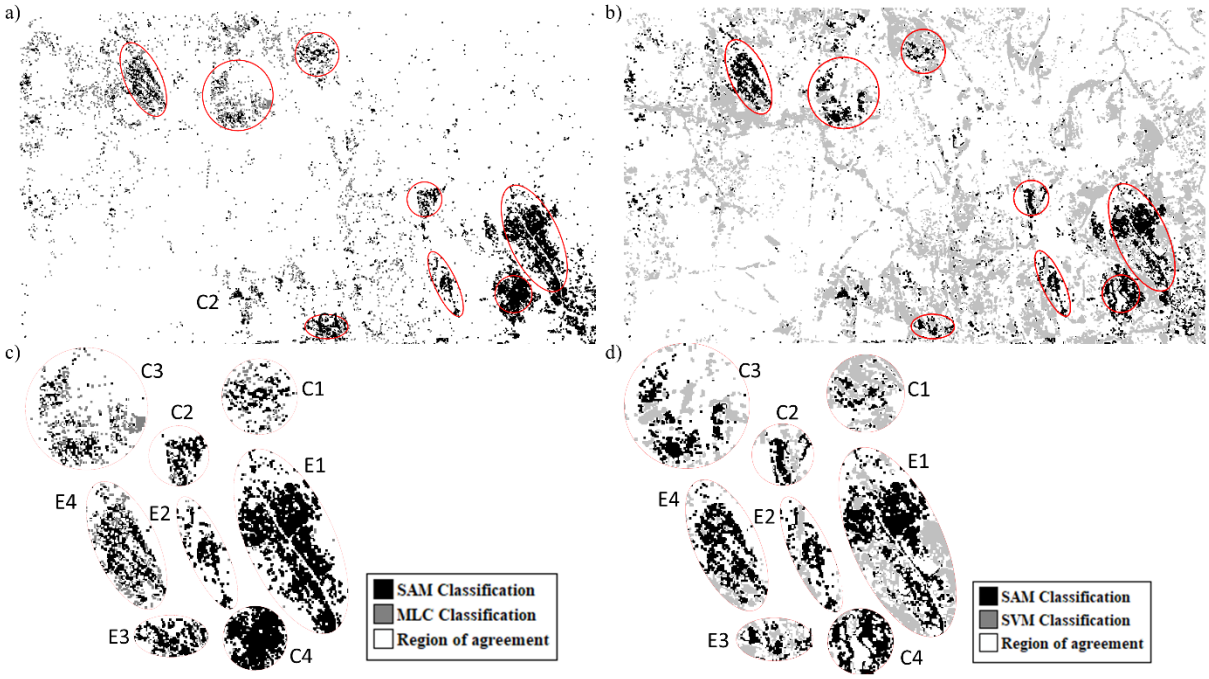


Figure 6: a) Difference image between SAM and MLC, b) difference image between SAM and SVM, c) juxtaposed regions for the SAM vs MLC difference image and d) juxtaposed regions for the SAM vs SVM difference image.

### 4.3.2. Quantitative analysis

In addition to the visual qualitative analysis of the classification agreement, area calculations were done for the white regions of agreement, black SAM classification and grey MLC or SVM classifications as shown in Figures 6a and 6b in subsection 4.3.1 above. Results in Table 3 show that the SAM and MLC classifications agreed in 94% pixels of the total study area of 393 $km^2$. It should be noted that this agreement was both for pompom-containing and non-pompom-containing pixels. Consistent with the qualitative analysis, the MLC only classified 0.22% of the study area as pompom-containing that was not classified as such by the SAM. However, SAM classified 5% of the study area as pompom-containing that was not classified as such by the MLC.

Table 3: Area percentages for the regions of agreement between SAM and MLC.

| | Spectral Angle Mapper vs. Maximum Likelihood | |
|---|---|---|
| | Area ($m^2$) | Percentage (%) |
| Region of agreement | 370 895 410 | 94,30 |
| SAM classification | 21 528 900 | 5,47 |
| MLC classification | 874 700 | 0,22 |
| Total | 393 299 010 | 100 |

Results in Table 4 show that the SAM and SVM classifications agreed in 75 % of pixels of the entire study area for both pompom and non-pompom classes. Unlike the MLC, SVM classified an area percentage of 21% as pompom-containing pixels that was not classified as such by the SAM method. In turn, the SAM also classified an area percentage of 4% as pompom-containing that was not classified as such by the SVM. These major differences are observable in Figures 5 and 6b. In general, the SVM classified many pixels as pompom-containing than both SAM and MLC but this can be attributed to commission errors committed by the SVM in wet grassy areas such as wetlands and riparian areas. The results in Tables 3 and 4 show that the MLC and SVM classifications were not quantitatively similar to the SAM classification within the 8 hotspots. Results of an independent SAM verification survey are discussed in subsection 4.4 below.

Table 4: Area percentages for the regions of agreement between SAM and SVM.

| | Spectral Angle Mapper vs. Support Vector Machine | |
|---|---|---|
| | Area ($m^2$) | Percentage (%) |
| Region of agreement | 293 926 410 | 74,73 |
| SAM classified | 16 123 500 | 4,10 |
| SVM classified | 83 249 100 | 21,17 |
| Total | 393 299 010 | 100 |

### 4.4.Generation of reference training samples

A total of 13 178 pixels were classified as pompom-containing by the SAM classifier and this resulted in 13 178 reference points for the pompom-containing pixels class. All the generated points could potentially be used as reference training samples in subsequent machine-learning classifications. However, it should be noted that the SAM classification was verified with a 92% mapping accuracy and so 1 in every 12 points in this reference dataset could be a misclassification (i.e., 8%). To generate a more accurate reference dataset, points from non-verified regions within the mapping area as well as points that were closer to misclassifications of the pixel-based accuracy assessment were manually removed in this study. As a result of this manual data cleaning exercise, a total of 9 178 points were removed from the pompom-containing reference dataset and only 4 000 points were retained. However, it should be noted that the manual deletion of points is not mandatory in this solution strategy as the deletion of some points does not improve the validity of the remaining points. For the non-pompom-containing class, 8 000 random points that are, at least, 100 m apart were generated within the non-pompom-containing class super-polygon. Figure 7 below shows 4 000 pompom-containing reference points in red together with the 8000 non-pompom-containing reference points in green.

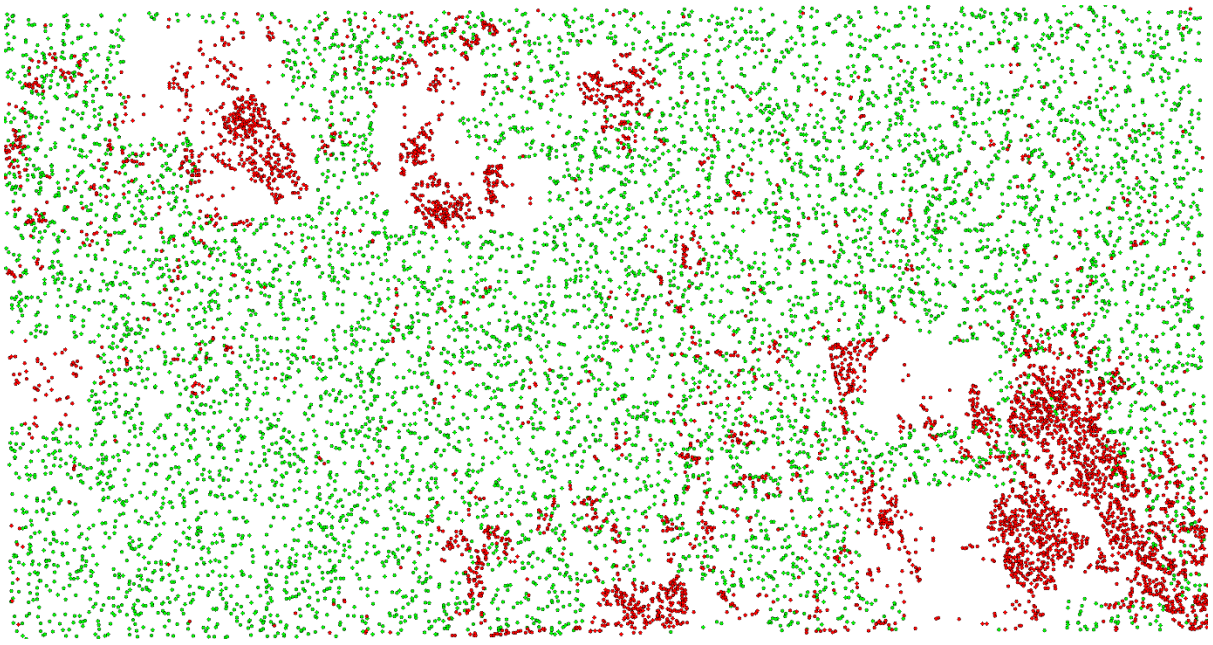

Figure 7: SAM classification derived reference training samples with 4 000 pompom reference points shown in red and 8 000 non-pompom reference points shown in green.

### 4.5.Verification of training samples

#### 4.5.1 Verification of the pompom-containing pixels class training samples

The pompom-containing training samples were verified using a set of 50 points selected from the SAM pompom-containing pixels class. Of the 50 selected points, 46 were verified meaning that the SAM classification was verified with a 92% overall mapping accuracy. The high accuracy could be attributed to the fact that most of the verification points were deliberately selected within very large clusters of pixels classified as pompom-containing as opposed to isolated pixels. This is because at the stage, it was not known whether SAM was accurate in mapping the pompom weed as the MLC and SVM classifiers produced different results within the SAM regions of high pompom density classification (i.e. the 8 hotspots). Of the four non-verified points, one fell on a burnt area that was burnt between image acquisition and the verification survey due to wildfires and thus could not be verified. The three remainder points consisted of the native *Senecio inornatus* plant which sometimes co-occurs with pompom weed as its native range includes grasslands (Egli *et al.*, 2020). It is suspected that one or more of the 20 endmembers used to train the SAM could have contained many *Senecio inornatus* plants within their 30 x 30 m boundary hence three isolated clusters of *Senecio inornatus* were committed into the pompom-containing pixels class by the SAM classifier. This, in future studies, can be avoided by not taking GCPs in areas where there is co-occurrence of the *Senecio inornatus* plant with the pompom weed. Figure 8 below shows the 46 verified points in green, three non-verified points that contained isolated clusters of *Senecio inornatus* in yellow, one non-verified point that could not be verified due to wildfires in red as well the 150 GCPs of the initial data collection survey in blue. As can be seen from Figure 8, the verification points were collected in areas that were not visited during the initial survey and were particularly collected in and around the Rietvlei Nature Reserve. Due to wildfires, some regions within the study area could not be included in the verification survey meaning that, in future studies, follow up verification surveys should be conducted during the rainy season.

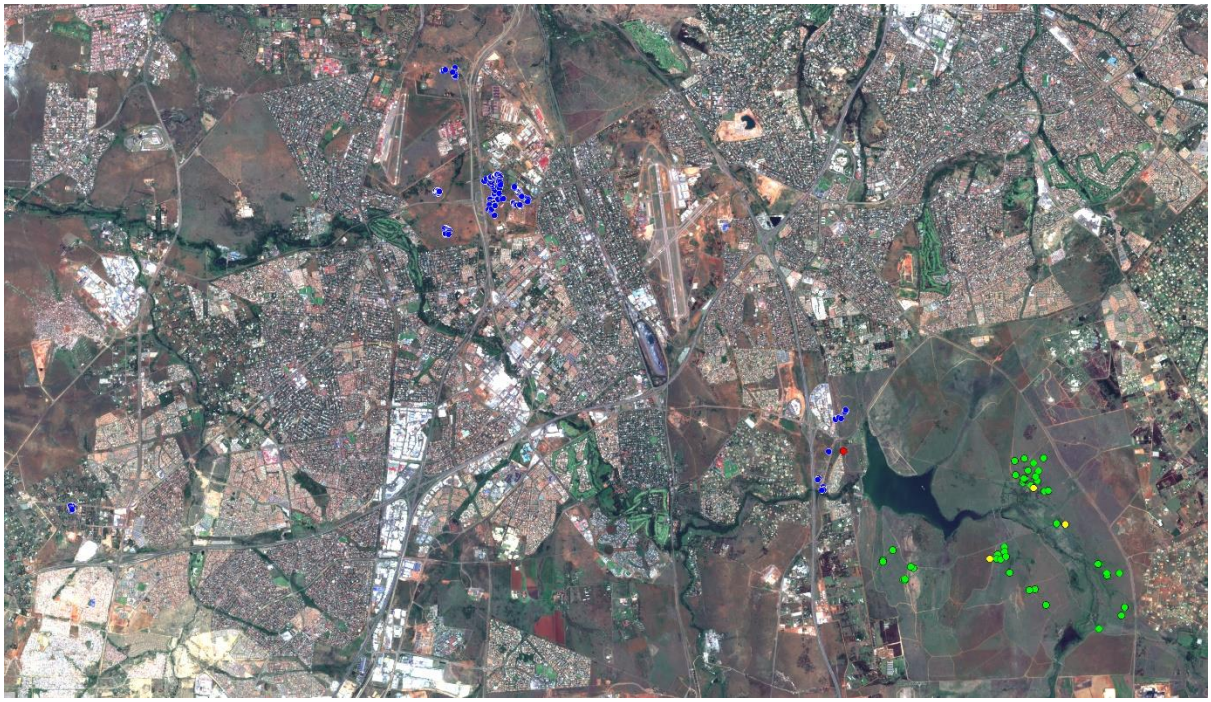

Figure 8: Sentinel 2 colour image used as a backdrop to show the 150 reference points in blue, 46 verified points in green, 3 non-verified *Senecio inornatus* points in yellow and 1 non-verified point in red.

### 4.5.2. Verification of the non-pompom-containing pixels class training samples

The non-pompom-containing pixels class of the SAM classification was verified using Google Earth images. Of the 140 non-pompom-containing samples, 125 were verified beyond doubt as belonging to the non-pompom-containing class as these fell in water bodies, highway roads, private golf courses, building rooftops, industrial buildings, open-cast mines and routinely monitored residential estates. It should be noted, however, that the 15 (~11%) non-verified points shown using 'U', for unverified, in Figure 9 below, are not misclassifications *per se* but were rather not verified as belonging to the non-pompom-containing class as these fell in open grass. Since pompom weed is known to affect grasslands, it could not be rule-out, beyond doubt, that these training samples do not belong to the pompom-containing pixels class.

Figure 9: 30 m DESIS colour image (R,G,B band combination 94, 59, 28) showing the 140 verification points with the Google Earth 'U' symbol above the 15 unverified non-pompom-containing training pixels.

## 5. Conclusion

This study presented a possible solution strategy for generating large numbers of the reference training samples sometimes required to train machine-learning algorithms in image processing of remotely sensed hyperspectral imagery. In particular, three strategically selected image classifiers, namely, SAM, MLC and SVM were assessed to investigate the best performing classifier for generating thousands of training samples for mapping the invasive pompom weed using 30 m DESIS hyperspectral imagery. The SAM, MLC and SVM classifiers had pixel-based classification accuracies of 87%, 73% and 67% for the pompom-containing pixels class, respectively. However, even though the region-based analysis revealed classification agreements of 94% and 75% between the SAM classification and the classifications of MLC and SVM methods, respectively, over the entire study area of 393 $km^2$, these classifiers produced different classification results within the SAM high pompom density classification regions of 4 circles and 4 ellipses (i.e., the 8 hotspots). This means neither MLC nor SVM classifications could be used to verify the SAM classification results both qualitatively and quantitatively. As a result, an independent verification survey had to be conducted at the Rietvlei Nature Reserve to validate the SAM pixel-based mapping accuracy. Results of this

study demonstrated that the SAM classifier can be used to generate a large number of accurate reference samples for training machine-learning algorithms to map pompom weed from DESIS hyperspectral data. A total of 4 000 pompom-containing and 8 000 non-pompom-containing training samples were generated from a SAM classification that was trained using only 20 endmembers. The training samples generated in this study will be used to produce labelled samples for training a robust machine-learning image classification algorithm that is based on a convolutional neural network (CNN) model for automated mapping of the invasive pompom weed in South Africa. Furthermore, this study presented a possible solution strategy to generate large numbers of accurate reference training samples for species-level mapping of IAPs in heterogenous environments from new generation spaceborne hyperspectral data using machine-learning algorithms.

**Acknowledgements**

The South African Department of Environment, Forestry, and Fisheries (DEFF) are thanked for funding noting that this publication does not necessarily represent the views or opinions of DEFF or its employees. We acknowledge the German Aerospace Center (abbreviated as DLR in its German name) for providing DESIS hyperspectral satellite data and in particular, Dr Rupert Müller for helping with the application, tasking requests and data downloading. We express our gratitude to Mr Phetole Manyama of the South African National Biodiversity Institute (SANBI) for his involvement on the conception of the research idea and identification of areas invaded by the pompom weed. We deeply thank Mr Phomolo Seriba for helping with the GNSS/RTK surveys as well as Mr Mcebisi Qabaqaba and Mr Luyolo Ziqu for helping with the fieldwork. We also thank the Rietvlei Nature Reserve management for giving us permission to conduct a verification survey on the park and in particular, Mrs Jeanri Weideman for helping with the research permit application process.

**Author contributions**

M.M., P.T., and T.Z. conceived the research idea. M.M. and P.T. conducted data collection and analysis, literature review. M.M., P.T., and A.R managed preparation of the manuscript, tables and figures. All the authors performed numerous manuscript editing.

## 6. References


Alonso, K. et al. (2019) 'Data products, quality and validation of the DLR earth sensing imaging spectrometer (DESIS)', Sensors (Switzerland), 19(20), pp. 1–44. doi: 10.3390/s19204471.

Bachmann, C.M., Donato, T.F., Lamela, G.M., Rhea, W.J., Bettenhausen, M.H., Fusina, R.A., Du Bois, K.R., Porter, J.H. and Truitt, B.R. (2002) Automatic classification of land cover on Smith Island, VA, using HyMAP imagery. IEEE Transactions on Geoscience and Remote Sensing, 40(10), pp. 2313-2330.

Costa, H., Foody, G. M. and Boyd, D. S. (2018) 'Supervised methods of image segmentation accuracy assessment in land cover mapping', Remote Sensing of Environment. Elsevier, 205(December 2017), pp. 338–351. doi: 10.1016/j.rse.2017.11.024.

Dennison, P. E., Halligan, K. Q. and Roberts, D. A. (2004) 'A comparison of error metrics and constraints for multiple endmember spectral mixture analysis and spectral angle mapper', Remote Sensing of Environment, 93(3), pp. 359–367. doi: 10.1016/j.rse.2004.07.013.

Dougherty, E. R., Newell, J. T. and Pelz, J. B. (1992) 'Morphological texture-based maximum-likelihood pixel classification based on local granulometric moments', Pattern Recognition, 25(10), pp. 1181–1198. doi: 10.1016/0031-3203(92)90020-J.

Egli, D. et al. (2020) 'DNA barcoding of endophagous immature stages elucidates the host-plant affinities of insects associated with the invasive *Senecio madagascariensis* in its native range in South Africa', Biological Control. Elsevier, 145(March), p. 104245. doi: 10.1016/j.biocontrol.2020.104245.

Fang, B. *et al.* (2020) 'Collaborative learning of lightweight convolutional neural network and deep clustering for hyperspectral image semi-supervised classification with limited training samples', ISPRS Journal of Photogrammetry and Remote Sensing. Elsevier, 161, pp. 164–178. doi: 10.1016/j.isprsjprs.2020.01.015.

Foody, G. (2008) 'Harshness in image classification accuracy assessment', International Journal of Remote Sensing, 29(11), pp. 3137–3158. doi: 10.1080/01431160701442120.

Foody, G. M. et al. (1992) 'Derivation and applications of probabilistic measures of class membership from the maximum-likelihood classification', Photogrammetric Engineering & Remote Sensing, 58(9), pp. 1335–1341.

Forsyth, G.G., Kruger, F.J. and Le Maitre, D.C. (2010) 'National veldfire risk assessment: Analysis of exposure of social, economic and environmental assets to veldfire hazards in South Africa'. National Resources and the Environment CSIR, Fred Kruger Consulting cc.

Goodall, J. et al. (2011) 'Are environmental factors important facilitators of pompom weed (*Campuloclinium macrocephalum*) invasion in South African rangelands?', Biological Invasions, 13(10), pp. 2217–2231. doi: 10.1007/s10530-011-0035-6.

Hamada, Y. et al. (2007) 'Detecting Tamarisk species (Tamarix spp.) in riparian habitats of Southern California using high spatial resolution hyperspectral imagery', Remote Sensing of Environment, 109(2), pp. 237–248. doi: 10.1016/j.rse.2007.01.003.

Hedling, G., A.Parker,, Wonnacott, R. (2000) 'TrigNet The Network of Active GPS Base Stations for South Africa', Proceedings of the 13th International Technical Meeting of the Satellite Division of The Institute of Navigation (ION GPS 2000), Salt Lake City, UT, September 2000, pp. 1865-1870.

Hu, X et al., (2022) '$S^3$ ANet: Spectral-spatial-scale attention network for end-to-end precise crop classification based on UAV-borne $H^2$ imagery' *ISPRS Journal of Photogrammetry and* Remote Sensing,183, pp. 147-163. d oi.org/10.1016/j.isprsjprs.2021.10.014

Huang, C., Davis, L. S., Townshend, J.R.G. (2002) 'An assessment of support vector machines for landcover classification', International Journal of Remote Seninsg, 23 (4), pp. 725-749. doi:1080/01431160110040323.

Huang, H. *et al.* (2020) 'The migration of training samples towards dynamic global land cover mapping', ISPRS Journal of Photogrammetry and Remote Sensing. Elsevier, 161, pp. 27–36. doi: 10.1016/j.isprsjprs.2020.01.010.

Huang, L., Chen, Y. and He, X. (2021) 'Weakly Supervised Classification of Hyperspectral Image Based on Complementary Learning', Remote Sensing, 13, pp5009. doi.org/10.3390/rs13245009

Kavzoglu, T. and Colkesen, I. (2009) 'A kernel functions analysis for support vector machines for land cover classification', International Journal of Applied Earth Observation and Geoinformation, 11(5), pp. 352–359. doi: 10.1016/j.jag.2009.06.002.

Kazmi, J.H., Haase, D., Shahzad, A., Shaikh, S., Zaidi, S.M. and Qureshi, S. (2021) Mapping spatial distribution of invasive alien species through satellite remote sensing in Karachi,

Pakistan: an urban ecological perspective. International Journal of Environmental Science and Technology, pp.1-18.

Kganyago, M. et al. (2018) 'Evaluating the capability of Landsat 8 OLI and SPOT 6 for discriminating invasive alien species in the African Savanna landscape', International Journal of Applied Earth Observation and Geoinformation. Elsevier, 67(January), pp. 10–19. doi: 10.1016/j.jag.2017.12.008.

Kruger, A. C. and Nxumalo, M. P. (2017) 'Historical rainfall trends in South Africa: 1921–2015', Water SA, 43(2), pp. 285–297. doi: 10.4314/wsa.v43i2.12.

Kruger, A. C. and Shongwe, S. (2004) 'Temperature trends in South Africa: 1960-2003', International Journal of Climatology, 24(15), pp. 1929–1945. doi: 10.1002/joc.1096.

Kruse, F. A. et al. (1993) 'The spectral image processing system (SIPS)-interactive visualization and analysis of imaging spectrometer data', Remote Sensing of Environment, 44(2–3), pp. 145–163. doi: 10.1016/0034-4257(93)90013-N.

Kutser, T. and Jupp, D. L. B. (2006) 'On the possibility of mapping living corals to the species level based on their optical signatures', Estuarine, Coastal and Shelf Science, 69(3–4), pp. 607–614. doi: 10.1016/j.ecss.2006.05.026.

Lawrence, R. L., Wood, S. D. and Sheley, R. L. (2006) 'Mapping invasive plants using hyperspectral imagery and Breiman Cutler classifications (Random Forest)', Remote Sensing of Environment, 100(3), pp. 356–362. doi: 10.1016/j.rse.2005.10.014.

Mafanya, M. et al. (2017) 'Evaluating pixel and object-based image classification techniques for mapping plant invasions from UAV derived aerial imagery: *Harrisia pomanensis* as a case study', ISPRS Journal of Photogrammetry and Remote Sensing, 129. doi: 10.1016/j.isprsjprs.2017.04.009.

Maxwell, A. E., Warner, T. A. and Fang, F. (2018) 'Implementation of machine-learning classification in remote sensing: An applied review', International Journal of Remote Sensing, 39(9), pp. 2784–2817. doi: 10.1080/01431161.2018.1433343.

McConnachie, A. J. et al. (2011) 'The initiation of a biological control programme against pompom weed, *campuloclinium macrocephalum* (Less.) DC. (Asteraceae), in South Africa', African Entomology, 19(2), pp. 258–268. doi: 10.4001/003.019.0217.

McGeoch, M. A. et al. (2010) ‘Global indicators of biological invasion: Species numbers, biodiversity impact and policy responses’, Diversity and Distributions, 16(1), pp. 95–108. doi: 10.1111/j.1472-4642.2009.00633.x.

Melgani, F. and Bruzzone, L. (2004) ‘Classification of hyperspectral remote sensing images with support vector machines’, IEEE Transactions on Geoscience and Remote Sensing, 42(8), pp. 1778–1790. doi: 10.1109/TGRS.2004.831865.

Miao, X., Patil, R., Heaton, J.S. and Tracy, R.C. (2011) ‘Detection and classification of invasive saltcedar through high spatial resolution airborne hyperspectral imagery’, International Journal of Remote Sensing, 32(8), pp.2131-2150.

Mirik, M. et al. (2013) ‘Remote distinction of a noxious weed (Musk Thistle: Carduus Nutans) using airborne hyperspectral imagery and the support vector machine classifier’, Remote Sensing, 5(2), pp. 612–630. doi: 10.3390/rs5020612.

Mountrakis, G., Im, J. and Ogole, C. (2011) ‘Support vector machines in remote sensing: A review’, ISPRS Journal of Photogrammetry and Remote Sensing. Elsevier B.V., 66(3), pp. 247–259. doi: 10.1016/j.isprsjprs.2010.11.001.

Müller, R. et al. (2016) ‘The new hyperspectral sensor desis on the multi-payload platform muses installed on the iss’, International Archives of the Photogrammetry, Remote Sensing and Spatial Information Sciences - ISPRS Archives, 2016-Janua(July), pp. 461–467. doi: 10.5194/isprsarchives-XLI-B1-461-2016.

Müllerová, J., Pergl, J. and Pyšek, P. (2013) ‘Remote sensing as a tool for monitoring plant invasions: Testing the effects of data resolution and image classification approach on the detection of a model plant species *Heracleum mantegazzianum* (giant hogweed)’, International Journal of Applied Earth Observation and Geoinformation, 25(1), pp. 55–65. doi: 10.1016/j.jag.2013.03.004.

Narumalani, S. et al. (2006) ‘A comparative evaluation of ISODATA and spectral angle mapping for the detection of saltcedar using airborne hyperspectral imagery’, Geocarto International, 21(2), pp. 59–66. doi: 10.1080/10106040608542384.

Nidamanuri, R. R. and Zbell, B. (2011) ‘Use of field reflectance data for crop mapping using airborne hyperspectral image’, ISPRS Journal of Photogrammetry and Remote Sensing.

International Society for Photogrammetry and Remote Sensing, Inc. (ISPRS), 66(5), pp. 683–691. doi: 10.1016/j.isprsjprs.2011.05.001.

Perumal, K. and Bhaskaran, R. (2010) 'Supervised Classification Performance of Multispectral Images', 2(2), pp. 124–129. Available at: http://arxiv.org/abs/1002.4046.

Rajapakse, S. S. et al. (2006) 'Identifying and classifying water hyacinth (*Eichhornia crassipes*) using the HyMap sensor', Remote Sensing and Modeling of Ecosystems for Sustainability III, 6298(September), p. 629804. doi: 10.1117/12.676265.

Sabat-Tomala, A., Raczko, E. and Zagajewski, B. (2020) 'Comparison of support vector machine and random forest algorithms for invasive and expansive species classification using airborne hyperspectral data', Remote Sensing, 12(3). doi: 10.3390/rs12030516.

Sahithi, V.S., Subbiah, S. and Agrawal, S. (2019) 'Comparison of Support Vector Machine, Artificial Neural Networks and Spectral Angle Mapper Classifiers on Fused Hyperspectral Data for Improved LULC Classification' . In 2019 8th International Conference on Modeling Simulation and Applied Optimization (ICMSAO) (pp. 1-6). IEEE.

Silva, A. F.; Barbosa, P. A.; Zimback, C. R. L.; Landim P. M. B. (2013) 'Geostatistics and remote sensing methods in the classification of images of areas cultivated with citrus', Engineering Agriculture, 33(6), 1245-1256.

Skowronek, S. et al. (2018) 'Transferability of species distribution models for the detection of an invasive alien bryophyte using imaging spectroscopy data', International Journal of Applied Earth Observation and Geoinformation, 68, pp. 61–72. doi: 10.1016/j.jag.2018.02.001.

Strahler, A. H. (1980) 'The use of prior probabilities in maximum likelihood classification of remotely sensed data', Remote Sensing of Environment, 10(2), pp. 135–163. doi: 10.1016/0034-4257(80)90011-5.

Tittensor, D. P. et al. (2014) 'Biodiversity Targets', Science, 346(6206), pp. 241–243.

Underwood, E., Ustin, S. and DiPietro, D. (2003) 'Mapping nonnative plants using hyperspectral imagery', Remote Sensing of Environment, 86(2), pp. 150–161. doi: 10.1016/S0034-4257(03)00096-8.

Ustin, S. L. et al. (2002) 'Hyperspectral remote sensing for invasive species detection and mapping', International Geoscience and Remote Sensing Symposium (IGARSS). IEEE, 3(C), pp. 1658–1660. doi: 10.1109/igarss.2002.1026212.

Wang, W., Dou, S. and Wang, S. (2019) ‘Alternately updated spectral-spatial convolution network for the classification of hyperspectral images’, Remote Sensing, 11(15).1794. doi: 10.3390/rs11151794.

Wilson, J. R. U. et al. (2018) ‘Indicators for monitoring biological invasions at a national level’, Journal of Applied Ecology, 55(6), pp. 2612–2620. doi: 10.1111/1365-2664.13251.

Yang, C., Everitt, J. H. and Murden, D. (2011) ‘Evaluating high resolution SPOT 5 satellite imagery for crop identification’, Computers and Electronics in Agriculture. Elsevier B.V., 75(2), pp. 347–354. doi: 10.1016/j.compag.2010.12.012.

Yu, K. *et al.* (2022) ‘Comparison of Classical Methods and Mask R-CNN for Automatic Tree Detection and Mapping Using UAV Imagery’, Remote Sensing,14(2),pp 295. doi.org/10.3390/rs14020295

Zengeya, T.A. and Wilson, J.R. (eds.) 2020. The status of biological invasions and their management in South Africa in 2019. pp.71. South African National Biodiversity Institute, Kirstenbosch and DSI-NRF Centre of Excellence for Invasion Biology, Stellenbosch. http://dx.doi.org/10.5281/zenodo.3947613

Zhu, G. and Blumberg, D. G. (2002) ‘Classification using ASTER data and SVM algorithms: The case study of Beer Sheva, Israel’, Remote Sensing of Environment, 80(2), pp. 233–240. doi: 10.1016/S0034-4257(01)00305-4.